Testing $f(R)$ gravity models with DESI-BAO and other cosmological data

Francisco Plaza[1, 2, *] and Lucila Kraiselburd[1, 2]

[1] *Facultad de Ciencias Astronómicas y Geofísicas, Universidad Nacional de La Plata, Observatorio Astronómico, Paseo del Bosque, B1900FWA La Plata, Argentina*

[2] *Consejo Nacional de Investigaciones Científicas y Técnicas (CONICET), Godoy Cruz 2290, 1425, Ciudad Autónoma de Buenos Aires, Argentina*

(Dated: March 2025)

In this paper, we conduct a statistical analysis of various cosmological models within the framework of $f(R)$ gravity theories, motivated by persistent challenges in modern cosmology, such as the unknown mechanisms driving the late-time accelerated expansion of the universe. We begin by presenting a comprehensive formulation of these theories and discussing their potential to resolve the outstanding issues. Following this, we perform a detailed statistical examination in a cosmological context, leveraging a wide array of observational data. Special attention is given to the incorporation of the latest Baryon Acoustic Oscillation (BAO) measurements from the Dark Energy Spectroscopic Instrument (DESI) and of the Pantheon$^+$+SH0ES compilation, which play a critical role in constraining these models. Our results show an increase in the values of the distortion parameter b and of the Hubble parameter H_0 estimates, due to the use of this new compilation of SnIa data. However, no major changes are perceived when using the DESI data set instead of the previous BAO observations.

I. INTRODUCTION

It has been known since 1998 that the universe is currently undergoing an accelerated expansion [1, 2]. This discovery led to the introduction of the cosmological constant in the standard model of cosmology, through its inclusion in the Einstein-Hilbert action to explain such accelerated expansion of the universe:

$$S = \frac{1}{2\kappa^2}\int d^4x\sqrt{-g}(R - 2\Lambda) + S_m(g_{\mu\nu}, \psi) \qquad (1)$$

where $\kappa^2 = \frac{8\pi G}{c^4}$

From this action, one obtains Einstein's field equations with the cosmological constant:

$$R_{\mu\nu} - \frac{1}{2}Rg_{\mu\nu} + \Lambda g_{\mu\nu} = \kappa^2 T_{\mu\nu} \qquad (2)$$

These field equations have successfully described this latest evolutionary stage of the universe. However, some concerns like the Hubble tension between Riess et al. [3] and Planck Collaboration [4] estimates, and the lack of understanding of the physical cause behind the accelerated expansion continue to motivate further studies on this phenomenon. This last issue arises from the ambiguity in the context of general relativity regarding whether the cosmological constant belongs to the right-hand side of the field equations, implying new forms of matter to be included in $T_{\mu\nu}$, or whether it belongs to the left-hand side, representing previously unknown aspects of spacetime.

From this interpretative problem, several proposals have emerged. Notably, if exotic matter were responsible for this phenomenon (for example, quintessence or k-essence fields [5–8]), it would constitute approximately 70% of the universe. Other proposals consist in assuming that the vacuum energy of quantum fields in the standard model of particle physics is the cause of the accelerated expansion and include it in the energy-momentum tensor; however, they provide the most inaccurate prediction in history, deviating by several orders of magnitude [9–11].

On the other hand, $f(R)$ theories constitute a promising alternative due to their ontological simplicity, proposing that the expansion is driven by the dynamics of spacetime itself. They represent previously unknown aspects of spacetime dynamics and curvature that become relevant at very large scales, without resorting to vacuum energy or unknown exotic species [12]. In this way, these theories provide a well-defined and plausible explanation of the physics underlying the epochs of accelerated expansion of the universe—something that remains unclear with the mere inclusion of the cosmological constant and its interpretation within the framework of standard cosmology. These unknown aspects of the gravitational interaction could originate from quantum phenomena intrinsic to gravity itself or from quantum corrections required for it, manifested in this context as part of an effective theory representing the low-energy limit of a more fundamental quantum theory of gravitation, or a unified theory of all fundamental interactions.[12–14]. Additionally, they are of significant theoretical interest, as they offer a framework in which both inflation and late-time acceleration may be unified within a single underlying mechanism [15, 16]. This is not achievable within the standard cosmological model, in which the use of a cosmological constant is not capable of explaining both stages of accelerated expansion and requires invoking ex-

*Electronic address: Fran22@fcaglp.unlp.edu.ar

otic entities—such as the inflaton field—to address early-universe problems, such as the flatness problem and the horizon problem.

This kind of models arise from a generalization of the action to one that includes a function $f(R)$ instead of just the Ricci scalar:

$$S = \frac{1}{2\kappa^2}\int d^4x\sqrt{-g}f(R) + S_m(g_{\mu\nu},\psi) \tag{3}$$

The metric formalism was employed, and the corresponding modified field equations were obtained:

$$f_R(R)R_{\mu\nu} - \frac{1}{2}f(R)g_{\mu\nu} - (\nabla_\mu\nabla_\nu - g_{\mu\nu}\Box)f_R(R) = \kappa^2 T_{\mu\nu} \tag{4}$$

where $f_R = \frac{df}{dR}$, $\Box$ is the d'Alembertian operator and ∇_μ is the covariant derivative.

In this context, all terms depend on the Ricci scalar, with the accelerated expansion of the universe attributed exclusively to the geometric aspects of spacetime. Even when assuming a vacuum state and $R = constant = R_0$, the dynamics correspond to a universe undergoing accelerated expansion [17], characterized by an effective cosmological constant given by:

$$\Lambda_{ef} = \frac{f(R_0)}{(f_R(R_0))^2} \tag{5}$$

This interpretation of $f(R)$ theories remains valid as long as there is no evidence for the hypothetical scalaron, a particle associated with the scalar field that appears when transitioning from the Jordan frame to the Einstein frame [18–20]. However, even if the scalaron truly exists, it represents an exotic yet more natural species that arises inherently from the gravitational theory itself and, even some authors dare to suggest the $f(R)$ theories as dark matter candidates as well [16, 21]. However, in the present work, dark matter is included as an additional species in the energy-momentum tensor, and it is not modeled as an effect arising from modified gravity. In contrast, dark energy is entirely replaced by these spacetime effects within the framework of $f(R)$ gravity. If dark matter were not included in the energy-momentum tensor, the model would fail to correctly describe the expansion rate of the universe.

The purpose of this work is to perform statistical analyses to establish bounds on the parameters of $f(R)$ models (Starobinsky, Hu-Sawicki, Exponential and Hyperbolic Tangent) using the most recent data from SnIa (with the inclusion of calibrated-Cepheid supernovae), cosmic chronometers and baryon acoustic oscillations. Such models have already been studied and constrained using both older data of this kind and other data such as X-ray and UV fluxes from quasars (AGN), redshift space distorsions (RSD), cosmic microwave background (CMB), etc.([22–31] and many others). The idea is then to compare our results with several of these recent estimates in order to analyze the consistency of the allowed parameter spaces.

The article is organized as follows: in Section II we write the Friedmann equations to be solved to obtain the dynamics of $f(R)$. There is also a summary of the viability conditions that the theory must satisfy and the four models to be analyzed are presented. Next, in Section III we describe the data chosen to perform the statistical analysis as well as the expressions that relate them to the theory. Our results are presented in Section IV and in the following Section, V, a comparison is made with previously published estimates. Finally the conclusions are in Section VI. The different methods used to solve the dynamic equations are found in Appendix A.

II. COSMOLOGICAL MODELS IN $f(R)$

The field equations governing gravity in $f(R)$ theories 4, also admit the FLRW cosmological metric as a solution in terms of the scale factor of the universe $a(t)$:

$$ds^2 = -c^2dt^2 + a^2(t)\left(\frac{dr^2}{1-Kr^2} + r^2d\Omega^2\right) \tag{6}$$

The modified Friedmann equations are obtained assuming a spatially flat universe and substituting this solution into equations 4:

$$-3H^2 = -\frac{1}{f_R}\left(\frac{8\pi G}{c^4}\rho_i + c^2\frac{Rf_R - f}{2} - 3H\dot{R}f_{RR}\right) \tag{7}$$

$$-2\dot{H} = \frac{1}{f_R}\left[\frac{8\pi G}{c^4}\left(\rho_i + \frac{P_i}{c^2}\right) + f_{RRR}\dot{R}^2 + \left(\ddot{R} - H\dot{R}\right)f_{RR}\right] \tag{8}$$

where $H = \frac{\dot{a}}{a}$ and $i = m, r$; being m the total matter component, including both dark and baryonic matter, and r referring to radiation. These equations are solved numerically.

A. Viable $f(R)$ theories

As is well known, $f(R)$ functions must satisfy a set of strict requirements [32, 33] to ensure that the associated theory meets the stability criteria for its solutions, successfully passes solar system tests, and provides a well-founded cosmological description consistent with observational data on the accelerated expansion of the universe, among other considerations. These conditions can be summarized and enumerated as follows:

1. **Positivity of the effective gravitational constant:** The derivative $f_R = \frac{df}{dR}$ must remain positive for $R \geq R_0 > 0$, where R_0 represents the Ricci scalar in the current epoch. This guarantees a positive effective gravitational constant ($G_{\text{eff}} = G/f_R$)

and the absence of unphysical local anti-gravity effects:

$$f_R > 0, \quad \text{for } R \geq R_0 > 0. \tag{9}$$

2. **Stability under perturbations:** To avoid Dolgov-Kawasaki instabilities, the second derivative $f_{RR} = \frac{d^2 f}{dR^2}$ must also remain positive:

$$f_{RR} > 0, \quad \text{for } R \geq R_0. \tag{10}$$

3. **Asymptotic behavior for large R:** Along with the previous condition, any viable model should recover the behavior of the ΛCDM model in the high curvature regime, ensuring compatibility with both late-time cosmology and local tests. This requirement essentially mandates that $f(R)$ asymptotically approaches the Einstein-Hilbert action for large values of R:

$$f(R) \approx R - 2\Lambda, \quad \text{for } R \gg R_0. \tag{11}$$

4. **Cosmological dynamics during the matter-dominated era:** The model must satisfy:

$$0 < \frac{R f_{RR}}{f_R}(r) < 1, \quad \text{at } r = -\frac{R f_R}{f} = -2, \tag{12}$$

which ensures that the modifications to General Relativity lead to a stable, ghost-free theory, and that the model can reproduce a cosmological evolution that mimics the standard matter-dominated era, followed by a smooth transition to an accelerating phase similar to what is observed in our universe.

To simplify the evaluation of these constraints, $f(R)$ models can be rewritten in a way that explicitly highlights deviations from ΛCDM. This is achieved by expressing them as:

$$f(R) = R - 2\Lambda y(R, b, \Lambda), \tag{13}$$

where $y(R, b, \Lambda)$ quantifies the deviation from the standard model, and b is the parameter controlling this deviation, the so-called *distortion parameter*. This formulation allows for a clearer connection between the modified model and the cosmological constant.

The condition for asymptotic behavior can then be re-expressed as:

$$\lim_{R\to\infty} f(R) = R + A, \tag{14}$$

where $A = -2\Lambda$, ensuring alignment with the ΛCDM model. This equivalence can be further expressed through the relation:

$$\Omega_{\Lambda,0}^{\Lambda CDM}(H_0^{\Lambda CDM})^2 = \Omega_{\Lambda,0}^{f(R)}(H_0^{f(R)})^2, \tag{15}$$

where the superscripts "ΛCDM" or "$f(R)$" denote parameters associated with the ΛCDM or $f(R)$ model, respectively, and the subscript 0 indicates the value at the present epoch. Furthermore, this formulation reveals that, at present, matter and radiation densities remain unchanged between ΛCDM and $f(R)$ models:

$$\Omega_{i,0}^{\Lambda CDM}(H_0^{\Lambda CDM})^2 = \Omega_{i,0}^{f(R)}(H_0^{f(R)})^2 = \frac{8\pi G}{3}\rho_{i,0}, \quad i = (m, r). \tag{16}$$

However, deviations from ΛCDM arise predominantly during late cosmic times, allowing for alternative explanations of the current accelerated expansion without invoking a fixed cosmological constant.

Parameters such $\Omega_{m,0}^{\Lambda CDM}$, b, $H_0^{\Lambda CDM}$ are used for fitting the models to observational data. Once fitted, the results are re-expressed in terms of $\Omega_{m,0}^{f(R)}$, b and $H_0^{f(R)}$ (from now on $\Omega_{m,0}$, b and H_0), which are derived using the equivalence relations mentioned earlier. This approach provides a comprehensive framework for assessing deviations from standard cosmology and their observational signatures.

B. The $f(R)$ theories

In this subsection, we present four of the most popular $f(R)$ gravity theories that satisfy all requirements outlined in the previous subsection and have been tested to date. Initially, each $f(R)$ function is introduced in its original formulation, followed by its reformulation into a more intuitive representation that aligns with the Einstein-Hilbert action. This approach highlights their potential to approximate the ΛCDM paradigm under appropriate conditions. The $f(R)$ theories studied in this work are:

i. Hu-Sawicki

The Hu-Sawicki theory, introduced in [34], presents a functional form for $f(R)$ gravity aimed at mimicking late-time cosmic acceleration:

$$f_{\rm HS}(R) = R - \frac{c_1 R_{HS}\left(\frac{R}{R_{HS}}\right)^{n_{\rm HS}}}{1 + c_2\left(\frac{R}{R_{HS}}\right)^{n_{\rm HS}}}, \tag{17}$$

where c_1 and c_2 are dimensionless constants, $n_{\rm HS}$ is a positive integer, and $R_{HS} \approx \Omega_{m0} H_0^2$. By redefining parameters as $c_1 R_{HS}/(2c_2) \equiv \Lambda$ and $b \equiv 2c_2^{1-1/n_{\rm HS}}/c_1$, the expression simplifies to:

$$f_{\rm HS}(R) = R - 2\Lambda\left[1 - \left\{1 + \left(\frac{R}{b\Lambda}\right)^{n_{\rm HS}}\right\}^{-1}\right]. \tag{18}$$

Here, Λ represents the cosmological constant, while b quantifies deviations from the ΛCDM paradigm. Viability conditions require $f_R > 0$ and $f_{RR} > 0$ for $R \geq R_0$, implying $b > 0$ when $n_{\rm HS}$ is odd.

ii. Starobinsky

Starobinsky's approach [12] modifies $f(R)$ as:

$$f_{\rm ST}(R) = R - \lambda R_S \left[1 - \left(1 + \frac{R^2}{R_S^2}\right)^{-n_S}\right], \qquad (19)$$

where $n_S > 0$, $\lambda > 0$, and $R_S \approx R_0$. Recasting this model in a comparable form, we define $\Lambda = \lambda R_S/2$ and $b = 2/\lambda$:

$$f_{\rm ST}(R) = R - 2\Lambda \left[1 - \left\{1 + \left(\frac{R}{b\Lambda}\right)^2\right\}^{-n_S}\right]. \qquad (20)$$

For $n_S = 1$, the Starobinsky theory aligns with the Hu-Sawickitheory at $n_{\rm HS} = 2$. Unlike the Hu-Sawicki theory, the Starobinsky formulation does not necessitate $b > 0$. Nonetheless, we assume $b > 0$ for simplicity in investigating deviations from ΛCDM.

iii. Exponential

The exponential theory [35] introduces a distinct parameterization:

$$f_{\rm E}(R) = R + \alpha\left[\exp(-\beta R) - 1\right], \qquad (21)$$

where $\alpha > 0$ and $\beta > 0$ ensure viability. Redefining parameters as $\Lambda = \alpha/2$ and $b = 2/(\alpha\beta)$, the function takes the form:

$$f_{\rm E}(R) = R - 2\Lambda\left[1 - \exp\left(-\frac{R}{b\Lambda}\right)\right]. \qquad (22)$$

In the limit $R \gg b\Lambda$, the theory asymptotically approaches $f(R) \sim R - 2\Lambda$, reproducing ΛCDM at high curvatures.

iv. Hyperbolic Tangent

Tsujikawa proposed an alternative [36]:

$$f_{\rm T}(R) = R - \xi R_T \tanh\left(\frac{R}{R_T}\right), \qquad (23)$$

where $\xi > 0$ and R_T are free parameters. This formulation offers unique phenomenological features distinct from other $f(R)$ models. The Hyperbolic Tangent theory introduces two key parameters, $\xi > 0$ and $R_T > 0$, which govern the model's behavior. By redefining these parameters in terms of $\Lambda = \xi R_T/2$ and $b = 2/\xi$, the functional form of $f(R)$ can be expressed as:

$$f_{\rm T}(R) = R - 2\Lambda \tanh\left(\frac{R}{b\Lambda}\right). \qquad (24)$$

This expression clearly demonstrates that as $b \to 0$ (corresponding to $\xi \to \infty$ and $R_T \to 0$, while ensuring ξR_T remains finite), the model asymptotically approaches the ΛCDM model

z	$H(z)$ (km s^{-1} Mpc^{-1})	Reference
0.09	69 ± 12	
0.17	83 ± 8	
0.27	77 ± 14	
0.4	95 ± 17	
0.9	117 ± 23	[37]
1.3	168 ± 17	
1.43	177 ± 18	
1.53	140 ± 14	
1.75	202 ± 40	
0.48	97 ± 62	[38]
0.88	90 ± 40	
0.1791	75 ± 4	
0.1993	75 ± 5	
0.3519	83 ± 14	
0.5929	104 ± 13	[39]
0.6797	92 ± 8	
0.7812	105 ± 12	
0.8754	125 ± 17	
1.037	154 ± 20	
0.07	69 ± 19.6	
0.12	68.6 ± 26.2	[40]
0.2	72.9 ± 29.6	
0.28	88.8 ± 36.6	
1.363	160 ± 33.6	[41]
1.965	186.5 ± 50.4	
0.3802	83 ± 13.5	
0.4004	77 ± 10.2	
0.4247	87.1 ± 11.2	[42]
0.4497	92.8 ± 12.9	
0.4783	80.9 ± 9	
0.75	98.8 ± 33.6	[43]

TABLE I: $H(z)$ values from the CC. Each column shows the redshift of the measurement, the $H(z)$ mean value (and its standard deviation) and reference, respectively.

III. OBSERVATIONAL DATA

In this section we summarize the observational data that we use to estimate the parameters of the $f(R)$ models presented above.

A. Cosmic chronometers

The cosmic chronometer (CC) method [37] is based on determining values of the Hubble parameter $H(z)$ for different redshifts through the study of the differential age evolution of ancient passive-evolving elliptical galaxies, which formed at the same time but are separated by a small redshift interval. Table I presents estimates of $H(z)$ obtained with this technique that we consider for this work.

B. Supernovae type Ia

Among the so-called "cataclysmic variables" there are some particularly energetic ones, the type Ia supernovae (SNeIa), which can be observed at large distances of up to z $\sim$ 2.3 so far. This group is chosen as one of the premier distance estimators due to the homogeneity of the spectra of these objects and their light curves, as well as the number of them distributed in all directions.

The distance module μ can be inferred both from the SNeIa data (being m_b an overall flux normalization and M_{abs} the absolute magnitude of the star)

$$\mu = m_b - M_{abs} \tag{25}$$

and through the following theoretical expression

$$\mu = 25 + 5\log_{10}(d_L(z)), \tag{26}$$

where d_L the luminosity distance

$$d_L(z) = (1+z)\int_0^z \frac{c}{H(z')}dz'. \tag{27}$$

In this article, we consider 1590 data from the Pantheon$^+$ compilation (PP)[44, 45] with $z > 0.01$. supplemented with 42 SNeIa calibrated by SH0ES Cepheids of the host galaxies [46](PPS). The addition of the latter means that it is not necessary to adopt a method to the analysis of absolute magnitude like the ones described in [29, 47–51]. Such that, the M_{abs} can be taken as a free parameter without having to add any further marginalization on it beyond that provided by SH0ES. Although these results have recently been questioned by the scientific community[52, 53], they have not been discarded and thus can be taken into account.

C. Baryon acoustic oscillations

The Baryonic Acoustic Oscillations (BAO) are a phenomenon that occurred before the decoupling of matter and radiation, when photons and baryons were strongly coupled through Thomson scattering, generating perturbations in the density of baryonic matter. These perturbations undergo oscillations that propagate as pressure waves because, on one hand, the presence of gravitational potentials increases the baryonic density, while on the other hand, the collisions between baryonic matter and radiation generate a decrease. When the temperature of the Universe is low enough for the decoupling of light with matter to occur (a stage known as the drag epoch z_d), the acoustic oscillations *freeze* , leaving a characteristic mark both in the cosmic microwave background and in the large-scale distribution of matter. The sound horizon at the drag epoch r_d is a characteristic scale given by the maximum distance that the acoustic wave could travel in the plasma before decoupling. It turns out that any overdensity of materia in the primordial plasma served as a seed for the birth of future galaxies. Therefore, it is worth noting that this characteristic scale is not only detected in the microwave background, but is also detected in the distribution of galaxies at the present time. In this way, BAOs can be used as a standard ruler for measuring cosmological distances.

We consider two collections of BAO data points obtained using different observational probes from a range of surveys. In the first one (BAO_1)(shown in Table II), we have collected 20 data from the SDSS [54–60] , DES [61] and the WiggleZ Dark Energy Survey [62] surveys ; and in the other, we have 12 measurements from DESI 2024 [63] survey (BAO_2). Something to keep in mind is that both compilations should not be used in their entirety in a single statistical analysis because the sky region and redshift range observed by DESI partially overlap with those previously studied whose observations are part of the BAO_1 group. Although the input catalog data used in the DESI and SDSS BAO analyses are different due to details of instrument performance and observing strategy, there are correlations between some of the shared objects which are larger at low redshifts. Some of the data between both compilations are in agreement but others do not, and the causes of these inconsistencies are still being discussed (although DESI data are supposed to be more accurate thanks to improvements in fitting processes and in raw data processing). Despite the fat that a single data set can be assembled by interleaving some data from each compilation (details in [63]), we decided to use each data set separately and analyze the estimates obtained for the different $f(R)$ models separately in order to compare them with each other.

The different BAO observables that are listed in Tables II and III [1] are defined by,

- Hubble distance $D_H(z)$,

$$D_H(z) = \frac{c}{H(z)} \tag{28}$$

- Diameter angular distance $D_A(z)$,

$$D_A(z) = \frac{1}{(1+z)}\int_0^z \frac{c}{H(z')}dz' \tag{29}$$

- Transverse comoving distance $D_M(z)$

$$D_M(z) = (1+z)D_A(z) \tag{30}$$

- Volume-averaged distance $D_V(z)$

$$D_V(z) = \left[(1+z)^2 D_A^2(z)\frac{cz}{H(z)}\right]^{1/3}. \tag{31}$$

[1] these distance measurements include the r_d^{fid}, the sound horizon at the drag epoch of each fiducial cosmology used in each observation.

$z_{\rm eff}$	Value	Observable	Reference
0.15	4.473 ± 0.159	D_V/r_d	[54]
0.44	11.548 ± 0.559	D_V/r_d	
0.6	14.946 ± 0.680	D_V/r_d	[62]
0.73	16.931 ± 0.579	D_V/r_d	
1.52	26.005 ± 0.995	D_V/r_d	[58]
0.81	10.75 ± 0.43	D_A/r_d	[61]
0.38	$10.272 \pm 0.135 \pm 0.074$	D_M/r_d	
0.51	$13.378 \pm 0.156 \pm 0.095$	D_M/r_d	[59]
0.61	$15.449 \pm 0.189 \pm 0.108$	D_M/r_d	
0.698	17.65 ± 0.3	D_M/r_d	[56]
1.48	30.21 ± 0.79	D_M/r_d	[57]
2.3	37.77 ± 2.13	D_M/r_d	[55]
2.4	36.6 ± 1.2	D_M/r_d	[60]
0.698	19.77 ± 0.47	D_H/r_d	[56]
1.48	13.23 ± 0.47	D_H/r_d	[57]
2.3	9.07 ± 0.31	D_H/r_d	[55]
2.4	8.94 ± 0.22	D_H/r_d	[60]
0.38	$12044.07 \pm 251.226 \pm 133.002$	Hr_d [km/s]	
0.51	$13374.09 \pm 251.226 \pm 147.78$	Hr_d [km/s]	[59]
0.61	$14378.994 \pm 266.004 \pm 162.558$	Hr_d [km/s]	

TABLE II: Distance bounds from BAO measurements of different observational probes and surveys. The table include the effective redshift of the measurement, the mean value and standard deviation, the observable and the reference.

$z_{\rm eff}$	D_M/r_d	D_H/r_d	r or D_V/r_d
0.295	—	—	7.93 ± 0.15
0.510	13.62 ± 0.25	20.98 ± 0.61	-0.445
0.706	16.85 ± 0.32	20.08 ± 0.60	-0.420
0.930	21.71 ± 0.28	17.88 ± 0.35	-0.389
1.317	27.79 ± 0.69	13.82 ± 0.42	-0.444
1.491	—	—	26.07 ± 0.67
2.330	39.71 ± 0.94	8.52 ± 0.17	-0.477

TABLE III: Distance constraints coming from BAO estimations published by DESI Collaboration [63]. The table shows the effective redshift (z_{eff}) of each measurement and, in some cases, both D_M/r_d and D_H/r_d quantities (which are correlated with a coefficient r); or D_V/r_d in the others.

IV. RESULTS

Here we present the results obtained for each $f(R)$ model from performing statistical analyzes using a Markov chain Monte Carlo method (emcee Python's library) and the observational data previously described in section III. The free parameters to be constrained are: the distortion parameter b, the total matter density parameter Ω_{m0}, the Hubble parameter H_0 and the absolute magnitud M_{abs}, the latter in cases where the SnIa observational data are used.

The parameter spaces estimated from the different analyses are detailed in Table V and Figures 2, 3, 4, 5, 6 and 7. The results obtained for the ΛCDM model are also added in Table IV and Fig. 1. Our results indicate that the BAO data restrict the allowed parameter spaces more than the PPS and CC data alone. Furthermore, it is observed that despite the smaller number of data, those of BAO coming from DESI (BAO_2) are a little more restrictive than those of BAO_1 (mostly being from the Sloan Digital Sky Survey), but the estimated spaces from both analyzes are consistent with each other. These behaviors are reflected both in the four $f(R)$ models studied in this article and in the standard cosmological model as well. On the other hand, the results obtained show that the data from Pantheon$^+$ shift and also increase the size of the distortion parameter b allowed space with respect to the previously results obtained using the Pantheon data [26–28] and that this fact is not due to the inclusion of the SnIa cepheid-calibrated SH0ES data[2], as can be seen in Fig. 2 for the Starobinsky model but that is also reflected in the other models. This issue will be described in the next section when comparing our findings with those of other authors. In addition, as has already been seen in other articles [28, 29] the intervals obtained for this parameter differ between the $f(R)$ models due to the different functional forms that each one has. However, the allowed estimated regions for the rest of the free parameters are consistent between the $f(R)$ models analyzed here. Finally, it is important to note that although $f(R)$ models do not seem to alleviate the H_0 tension, they do not exhibit a greater tension than the standard model in fits such as the one presented in this work, which relies on late-universe data and the model-independent estimate by Riess[46].

A. The Starobinsky model

From the results presented in Table V and Fig. 3, it is clear that in addition to further restricting the parameter spaces, both BAO data groups generate correlations between b and H_0, and between b and the M_{abs} that are

[2] The use of these data points generates quite considerable shifts in the 1D posteriors towards higher values of both H_0 and M_{abs}

Model	Data	H_0	Ω_{m0}	M_{abs}
ΛCDM	CC+PPS	$71.604^{+0.822(1.678)}_{-0.936(1.745)}$	$0.324^{+0.014(0.030)}_{-0.017(0.031)}$	$-19.295^{+0.024(0.047)}_{-0.026(0.052)}$
	CC+PPS+BAO_1	$70.657^{+0.466(1.100)}_{-0.685(1.162)}$	$0.319^{+0.009(0.019)}_{-0.010(0.019)}$	$-19.326^{+0.017(0.037)}_{-0.020(0.036)}$
	CC+PPS+BAO_2	$71.016^{+0.610(1.057)}_{-0.488(1.084)}$	$0.314^{+0.010(0.021)}_{-0.010(0.021)}$	$-19.317^{+0.018(0.033)}_{-0.015(0.034)}$

TABLE IV: ΛCDM results from statistical analysis using different datasets (Cosmic Chronometers (CC), SneIa from Pantheon$^+$+SH0ES (PPS) Collaborations, and several datasets from BAOs (BAO_1 and BAO_2)). For each parameter, we present the mean value and the 68% (95%) confidence levels or the upper limits obtained.

Model	Data	b	H_0	Ω_{m0}	M_{abs}
Starobinsky	CC+PP	$1.847^{+1.159(1.912)}_{-0.865(1.769)}$	$67.374^{+1.758(3.088)}_{-1.343(2.114)}$	$0.302^{+0.024(0.058)}_{-0.038(0.072)}$	$-19.415^{+0.056(0.129)}_{-0.040(0.093)}$
	CC+PPS	$2.498^{+0.799(1.335)}_{-0.970(2.014)}$	$71.464^{+1.064(2.221)}_{-1.018(2.828)}$	$0.267^{+0.033(0.067)}_{-0.024(0.052)}$	$-19.289^{+0.026(0.062)}_{-0.027(0.065)}$
	CC+PPS+BAO_1	$0.531^{+0.520(1.148)}_{-0.354(0.531)}$	$70.169^{+0.545(1.599)}_{-1.058(1.929)}$	$0.318^{+0.012(0.026)}_{-0.010(0.027)}$	$-19.336^{+0.018(0.047)}_{-0.026(0.056)}$
	CC+PPS+BAO_2	$0.618^{+0.511(1.285)}_{-0.432(0.618)}$	$70.441^{+0.610(1.667)}_{-1.073(2.117)}$	$0.312^{+0.014(0.029)}_{-0.009(0.027)}$	$-19.328^{+0.018(0.044)}_{-0.025(0.057)}$
Hu-Sawicki	CC+PPS	$0.660^{+0.315(0.535)}_{-0.297(0.649)}$	$71.430^{+0.645(1.746)}_{-1.109(2.461)}$	$0.261^{+0.038(0.067)}_{-0.011(0.018)}$	$-19.292^{+0.016(0.044)}_{-0.032(0.068)}$
	CC+PPS+BAO_1	$0.061^{+0.155(0.376)}_{-0.048(0.061)}$	$70.369^{+0.502(1.383)}_{-1.102(2.306)}$	$0.318^{+0.010(0.025)}_{-0.011(0.027)}$	$-19.333^{+0.015(0.044)}_{-0.031(0.068)}$
	CC+PPS+BAO_2	$0.021^{+0.174(0.398)}_{-0.015(0.021)}$	$70.943^{+0.201(1.092)}_{-1.289(2.399)}$	$0.314^{+0.009(0.026)}_{-0.014(0.030)}$	$-19.318^{+0.008(0.065)}_{-0.033(0.036)}$
Exponential	CC+PPS	$2.078^{+0.626(1.175)}_{-0.680(1.645)}$	$71.503^{+1.104(2.913)}_{-1.060(2.913)}$	$0.282^{+0.035(0.065)}_{-0.030(0.066)}$	$-19.288^{+0.026(0.062)}_{-0.027(0.062)}$
	CC+PPS+BAO_1	$1.298^{+0.437(0.695)}_{-0.513(1.160)}$	$70.073^{+0.765(1.921)}_{-0.744(1.552)}$	$0.320^{+0.012(0.027)}_{-0.010(0.026)}$	$-19.334^{+0.022(0.051)}_{-0.020(0.045)}$
	CC+PPS+BAO_2	$1.370^{+0.422(0.740)}_{-0.369(0.948)}$	$70.465^{+0.685(1.705)}_{-0.769(1.638)}$	$0.315^{+0.013(0.030)}_{-0.010(0.027)}$	$-19.322^{+0.018(0.044)}_{-0.021(0.046)}$
Hyperbolic tangent	CC+PPS	$3.979^{+0.660(1.020)}_{-1.325(2.846)}$	$71.487^{+1.145(2.270)}_{-0.559(1.773)}$	$0.289^{+0.036(0.065)}_{-0.024(0.060)}$	$-19.288^{+0.029(0.061)}_{-0.018(0.051)}$
	CC+PPS+BAO_1	$2.938^{+0.143(0.417)}_{-1.235(2.471)}$	$70.130^{+0.947(2.076)}_{-0.370(1.189)}$	$0.321^{+0.010(0.023)}_{-0.011(0.028)}$	$-19.331^{+0.024(0.052)}_{-0.014(0.039)}$
	CC+PPS+BAO_2	$3.082^{+0.211(0.548)}_{-1.001(2.293)}$	$70.561^{+0.828(1.736)}_{-0.368(1.178)}$	$0.317^{+0.010(0.024)}_{-0.012(0.028)}$	$-19.318^{+0.022(0.047)}_{-0.013(0.036)}$

TABLE V: Confidence intervals (68% and 95% levels) for the $f(R)$ models (Starobinsky, Hu-Saswicki, Exponential and Hyperbolic Tangent) obtained using the different groups of observables selected to perform the statistical analyses. (Cosmic Chronometers (CC), SneIa Pantheon$^+$+SH0ES (PPS) Collaboration and two different datasets from BAO (BAO_1 and BAO_2)).

not as visible when only CC and SnIa (PPS) are used. Also, the inclusion of these data reduces the degeneracies between the distortion parameter and Ω_{m0}. On the other hand, the 1D posteriors of parameters b, H_0 and M_{abs} are shifted towards lower values, while for Ω_{m0} it is shifted towards higher values. This last shift is contrary to what is perceived in the standard cosmological model. Furthermore, our findings using the BAO_1 data compilation are very similar to those obtained using BAO_2 with the exception that the latter are much less.

Finally, the b values reported in all the statistical analyzes carried out are not consistent with zero (ΛCDM) at 1σ but they are at 2σ only when the BAO data are included with the CC+PPS data sets. The estimates obtained for the remaining parameters are consistent with those from the ΛCDM model at 1σ with the exception of Ω_{m0} intervals in the CC+PPS case where they are at 2σ.

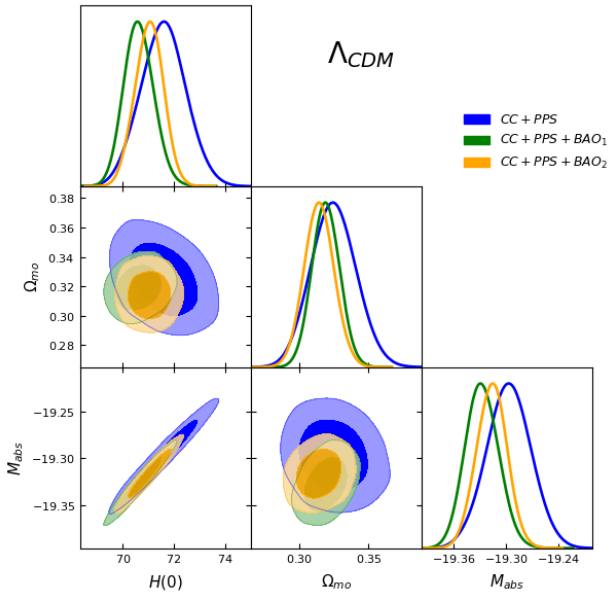

FIG. 1: Results for the matter density Ω_{m0}, the Hubble parameter H_0 and the absolute magnitud M_{abs} for the ΛCDM model using combinations of the Cosmic Chronometers, SneIa from Pantheon$^+$+SH0ES Collaborations, and two different datasets from BAO (BAO_1 and BAO_2). The plots show the 68% and 95% confidence regions.

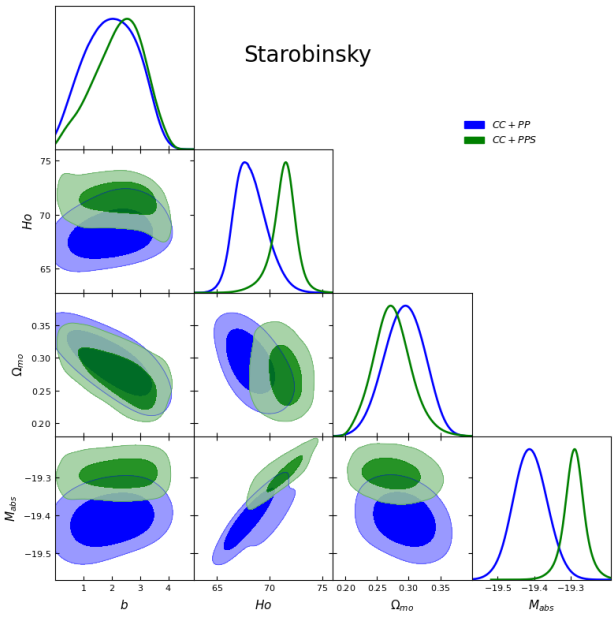

FIG. 2: Results of statistical analysis of $f(R)$ Starobinsky model with and without using the cepheid-calibrated SnIa by SH0ES. The darker and brighter regions represent 1σ (68 %) and 2σ (95%) confidence intervals, respectively

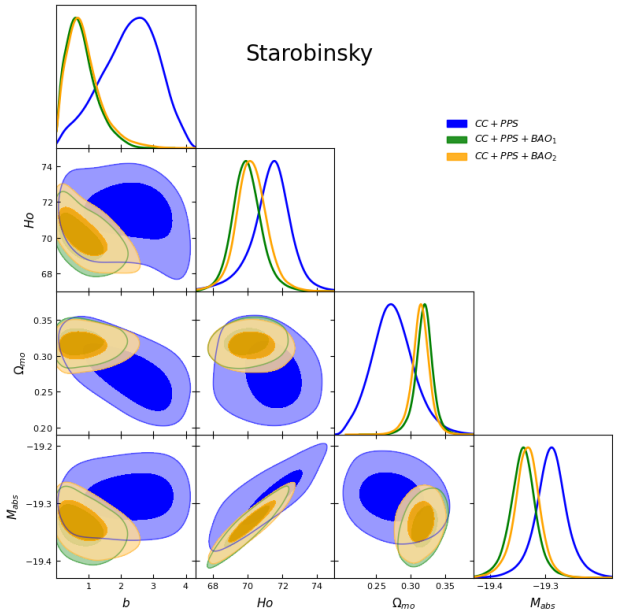

FIG. 3: Results of statistical analysis of $f(R)$ Starobinsky model with different combinations of the data sets. The darker and brighter regions represent 1σ (68 %) and 2σ (95%) confidence intervals, respectively

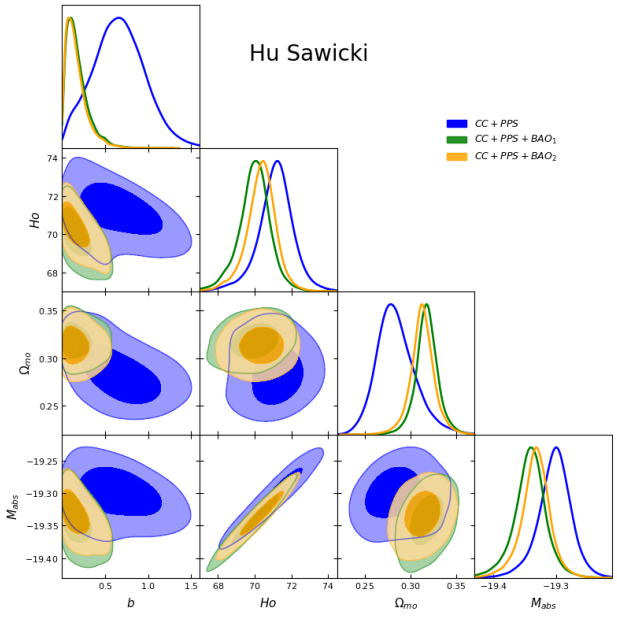

FIG. 4: Results of statistical analysis of $f(R)$ Hu Sawicki model with different combinations of the data sets. The darker and brighter regions represent 1σ (68 %) and 2σ (95%) confidence intervals, respectively

B. The Hu-Sawicki model

This model exhibits a very similar behavior to that previously analyzed, both with respect to the restriction

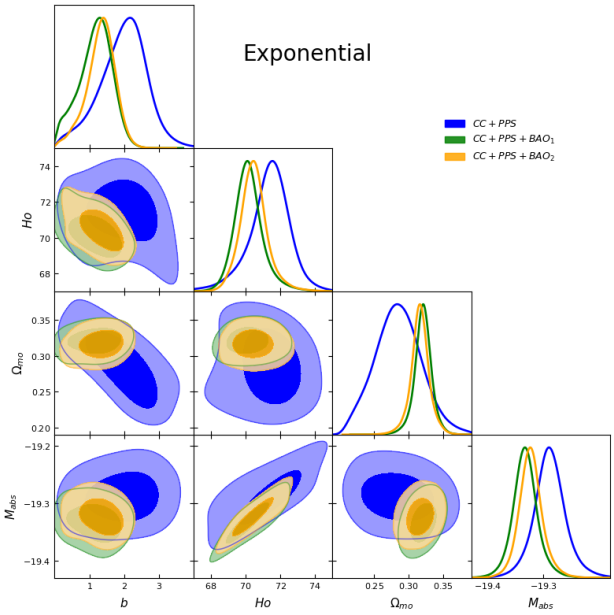

FIG. 5: Results of statistical analysis of $f(R)$ Exponential model with different combinations of the data sets. The darker and brighter regions represent 1σ (68 %) and 2σ (95%) confidence intervals, respectively

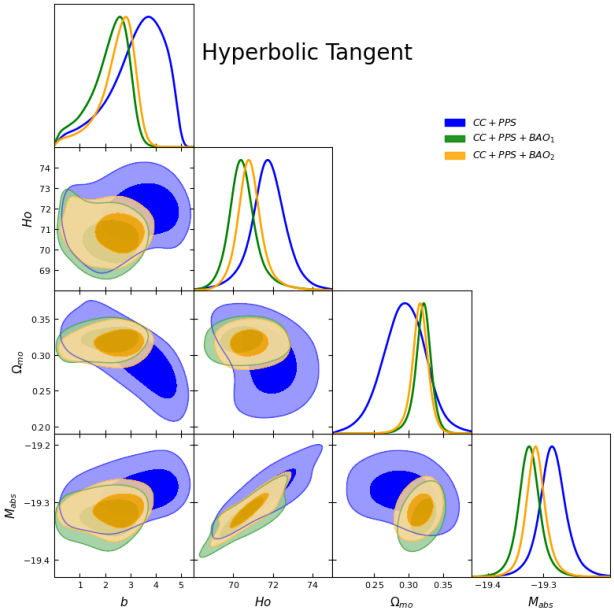

FIG. 6: Results of statistical analysis of $f(R)$ Hyperbolic Tangent model with different combinations of the data sets. The darker and brighter regions represent 1σ (68 %) and 2σ (95%) confidence intervals, respectively

power of the BAO data (including the very minor differences between the two BAO data sets), and to the regions obtained for the free parameters, the shifts of their 1D posterior distributions depending on the data sets used and the correlations between them with the exception of the distortion parameter b (Fig. 7). For this one, the allowed zone is smaller than that obtained for the Starobinsky case, and closer to the null value (it is consistent with this value at 2σ in the CC+PPS+BAO$_{1/2}$ analyses and almost also in the CC+PPS case). Since the Starobinsky model is equivalent to a Hu-Sawicki with $n = 2$, it could be inferred that the higher the value of n, the greater the shift of the 1D probability posterior towards non-null values for b.

Lastely, the results obtained for Ω_{m0}, H_0 and M_{abs} are consistent at 1σ with those reported for the ΛCDM model for all analyses except in the CC+PPS case, where Ω_{m0} interval is compatible 2σ.

C. The Exponential model

A clear difference between the above models and this one is that the estimated intervals for the distortion parameter b are larger in the Exponential model. This is understandable since due to the functional form of this $f(R)$, a larger value of b is needed in order to differentiate it from the ΛCDM model. However, the intervals obtained for the other free parameters are consistent with those of the previous models, perceiving the same types of correlation, 1D posterior distribution shifts and behaviors.

An interesting point to keep in mind is that although the results for parameter b are not consistent with ΛCDM at 2σ in any of the analyses, the estimated values for the other parameters are consistent at 1σ.

D. The Hyperbolic Tangent model

As in the previous case, the functional form of this model causes the intervals obtained for the distortion parameter to be shifted towards higher values. In addition, the shifts in the 1D posterior distributions and correlations of the parameters are very similar to those described for the other models, with the exception that, in this case, there is no defined correlation between the distortion parameter b and M_{abs}, and between b and H_0 as seen in the other $f(R)$ models.

Finally, as in the Exponential model, although the estimated interval for b is not consistent with the null value at 2σ, there is consistency between the regions obtained for the other parameters and the regions calculated for ΛCDM at 1σ.

E. Model comparison

We use different statistical criteria in order to determine which of the models presented in this article is the preferred one for the chosen data. The minimum value ofthe chi-square (χ^2) is defined in relation

to the maximum likelihood as $\chi^2_{min} = -2\ln\mathcal{L}_{max}$, while $\chi^2_\nu = \chi^2_{min}/\nu$ is the reduced chi-square being $\nu = N - k$ the number of degrees of freedom, N the total number of data points and k the number of free parameters of the model. We also take into account the Akaike (AIC) [64] and Bayesian (BIC) [65], [66] information criterions that are given by

$$\mathrm{AIC} = -2\ln\mathcal{L}_{max} + 2k \tag{32}$$

$$\mathrm{BIC} = -2\ln\mathcal{L}_{max} + k\ln N \tag{33}$$

It is assumed that the model with the lowest values of χ^2_{min}, AIC and BIC, is the one that best fits the data statistically. In contrast, in the case of reduced chi-square, the model most favored by the data is the one with an χ^2_ν value closest to 1. If this value is $>> 1$, the model is considered to be poor and therefore is subfitted while if it is $<< 1$, the model is overfitted either because it is not adequate to fit for noise, or the error variance is overestimated [67]. Among these statistical criteria, the χ^2_{min} is the only one that does not consider the number of free parameters of the model to be analyzed. This point is very important since for a nested model, the greater the number of parameters, the greater the likelihood, without taking into account the relevance of the new parameters included. Conversely, the other criteria do penalize the models that include more free parameters and they do so in different ways, with the BIC being the most severe of the three. This sometimes leads to the criteria having discrepancies between them and it is necessary to analyze whether the assumptions of the criteria are being violated ([66], [68] and many others). On the other hand, the comparison of criteria of two models is carried out by subtracting the values obtained by both models ($\Delta X = \Delta AIC$ or $\Delta X = \Delta BIC$) such that: a) if $0 \leq \Delta X \leq 2$ or $-2 \leq \Delta X < 0$ the evidence is weak, it cannot be defined which is better; b) if $2 < \Delta X \leq 6$ or $-6 \leq \Delta X < -2$ the evidence is positive; c) if $6 < \Delta X \leq 10$ or $-10 \leq \Delta X < 6$ the evidence is strong; and d) if $\Delta X > 10$ or $\Delta X < -10$ the evidence is very strong.

From the results shown in Table VI and the description above, it can be seen that the data combination CC+PPS+BAO$_2$ generates higher likelihoods for the models analyzed than the combination CC+PPS+BAO$_1$. For the Starobinsky model for both data combinations is given that although the χ^2_{min} are lower and χ^2_ν more closer to one than those of ΛCDM, the AIC and BIC are not, where the evidence is weak and strong in favor of the standard model of cosmology respectively. Meanwhile, for the Hu-Sawicki model, only for the CC+PPS+BAO$_1$ data set the χ^2_{min} is lower compared to the one from ΛCDM. For both data combinations χ^2_ν are more closer to one, but the AIC and BIC values are higher causing the evidence to be favorable to ΛCDM in a weak and strong way respectively. Finally from the values obtained for the the Exponential and Hyperbolic Tangent models it follows that for both data compilations the χ^2_{min} reach lower values than those of ΛCDM as well as lower AIC values, obtaining weak evidence supporting these $f(R)$ for the case CC+PPS+BAO$_1$ and furthemore, positive evidence for the case CC+PPS+BAO$_2$. However, this does not occur when both the results for χ^2_ν and BIC are analyzed. The χ^2_ν values are less close to 1 than those reported for the standard model, while the BIC are higher such that the evidence benefiting ΛCDM is positive when CC+PPS+BAO$_1$ is used, positive for the Exponential model in the case of CC+PPS+BAO$_2$ and weak for the Hyperbolic Tangent model for the same data set.

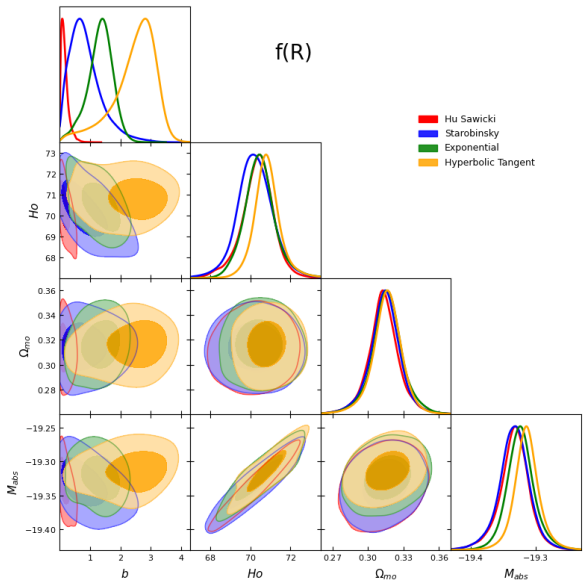

FIG. 7: Results of all the $f(R)$ models studied in this work employing CC +Pantheon$^+$ +SH0ES +BAO$_2$(DESI) data sets. The darker and brighter regions represent 1σ (68 %) and 2σ (95 %) confidence intervals, respectively.

V. DISCUSSION

In this section we compare our results with those published by other authors for the same $f(R)$ models with the same data but different developments and with similar data. Our analysis shows that the use of data from the Pantheon$^+$ compilation increases the size and shifts the 1D distribution towards higher values of the distortion parameter b. This can also be seen when comparing our results with those obtained in [26–28] (among many others) where Pantheon data were used and with those published in [29, 51, 69] where the previous data were replaced by Pantheon$^+$. However, this effect is not reflected in [70], but this is because in said analysis only the approximations developed by Basilakos [71] were used to obtain the expressions of $H(z)$ for the Hu-Sawicki and Starobinsky models. This procedure, being a perturbative method around ΛCDM, is not appropriate for

Data	Model	χ^2_{min}	χ^2_ν	AIC	BIC	ΔAIC	ΔBIC
CC+PPS+BAO$_1$	ΛCDM	1536.492	0.9615	1542.492	1558.627	-	-
	Starobinsky	1535.791	0.9617	1543.791	1565.304	1.299	6.677
	Hu-Sawicki	1536.373	0.9620	1544.373	1565.887	1.881	7.259
	Exponential	1534.157	0.9606	1542.157	1563.671	-0.334	5.043
	Hyperbolic Tangent	1533.201	0.9600	1541.201	1562.715	-1.290	4.088
CC+PPS+BAO$_2$	ΛCDM	1525.200	0.9592	1531.200	1547.320	-	-
	Starobinsky	1524.382	0.9593	1532.382	1553.876	1.183	6.556
	Hu-Sawicki	1525.217	0.9599	1533.217	1554.711	2.018	7.391
	Exponential	1520.897	0.9571	1528.897	1550.390	-2.303	3.070
	Hyperbolic Tangent	1519.370	0.9562	1527.370	1548.863	-3.830	1.543

TABLE VI: Results of standard statistical tools commonly used to assess model fitting: the chi-square and the reduced chi-square statistics (χ^2_{min}, χ^2_ν), the Akaike Information Criterion (AIC), and the Bayesian Information Criterion (BIC) for each model.

exploring regions of the distortion parameter b greater than one such as those presented when using Pantheon$^+$ compilation. On the other hand, the addition of cepheid-calibrated supernovae by the SH0ES collaboration to the Pantheon$^+$ compilation results in estimated values for H_0 and M_{abs} being higher than those estimated when using Pantheon$^+$ data alone.

Our estimates for the Starobinsky and Hu-Sawicki models using CC+PPS data are consistent at 1σ with those published in [51] for the CC+PPM[3] data sets. The small differences between the intervals found may be due to the fact that in one case calibrated supernovae with Cepheids by the SH0ES collaboration were used (PPS compilation) while in the other an statistical marginalization on the M_{abs} obtained from the SH0ES data was used (PPM).

There is also 1σ consistency with the results reported by [29] for the four $f(R)$ models using PPS+CC, PPS+CC+BAO$_1$ and PPS+CC+BAO$_2$ data sets, although the BAO data points are not exactly the same (in addition to not containing the DESI data). This paper also uses in some of ther analysis data from HII regions of galaxies, and parameters obtained from CMB data, such as the acoustic scale l_A^{Pl}, the displacement parameter R_A^{Pl} and the present baryon density $\omega_b^{Pl} = \frac{1}{4}\Omega_b h^2$. The latter, are estimated through a statistical analysis where a ΛCDM is taken as a fiducial model. So, like the authors of [26], we consider that despite being a datum that has a greater restrictive power than BAO, its use for testing alternative cosmological models is not the most appropriate [4]. Furthermore, it is not clear whether the authors use the entire data compilation provided by Pantheon$^+$ or exclude those with $z < 0.01$ where the sensitivity of the SnIa peculiar velocities is very large and so are their uncertainties (details in [44, 72] and a private communication with D. Brout). This last issue is also reflected in the analysis of the Exponential model performed by Odinstov et al.[69] where they also use the Pantheon$^+$ data (without SH0ES data or other H_0 estimates or marginalizations on M_{abs}), cosmic chronometers and CMB data described above. In addition, they incorporate the DESI data to previous BAO observations, but this should be done taking into account the suggestions explained in the DESI collaboration paper [63] that were ignored. Only their Ω_{m0} result is consistent at 1σ with ours. This is mainly due to the use of SH0ES and CMB data [5], since when comparing the estimates reported by [29] without SH0ES with those of [63] there is also consistency between the rest of the parameters.

VI. CONCLUSIONS

In this article we have studied four of the most popular $f(R)$ models (Starobinsky, Hu-Sawicki, Exponential and Hyperbolic Tangent) in a cosmological context. To

[3] PPM refers to the Pantheon$^+$ data compilation with a marginalization on the M_{abs} proposed by Camarena & Marra [49]

[4] In addition, another issue to consider is that if the H_0 estimate obtained with CMB data (without using H_0 estimates from SH0ES and/or no marginalization on the M_{abs} from said collaboration) is not consistent with the result published by SH0ES Collaboration, it is not correct to carry out a statistical study incorporating both data at the same time.

[5] The first data set generates a shift of the 1D posterior distribution of H_0 towards higher values, and a slight shift towards lower values in the case of parameter b; while the second, triggers a slight shift of the 1D posterior distribution of b towards higher values, and a shift towards lower values of H_0.

accomplish this, we have solved the modified Friedmann equations and carried out statistical analyses considering the most recent datasets from SnIa, BAO and CC so as to set bounds on the free parameters of the models.

We consider in this work the latest SnIa data compilation, which incorporates 42 SnIa data points calibrated with the Cepheids analyzed by the SH0ES collaboration [44, 45]. This allows us to avoid using a marginalization on the M_{abs}. Furthermore, we also use the BAO data provided by the DESI collaboration [63] last year. Because some of these data are correlated with certain data points published by the SLOAN collaboration, they cannot be used together, so we decided to use them in separate analyses and compare the results. Our estimates show that the Pantheon$^+$ data widen the b distortion parameter spaces of the four models compared to those obtained with previous SnIa compilations, while shifts towards higher 1D posteriors of the Hubble parameter are perceived due to the addition of the SH0ES data (not being consistent at 2σ with the value reported by Planck collaboration [4]). Although these data have been challenged by some authors [52, 53], to this day they remain valid, even more there are numerous H_0 estimates subsequent to these questions which are consistent with them [31, 73, 74]. So, it is entirely legitimate to use them to test the consistency of the models. On the other hand, the data from BAO continue to be the most restrictive and no major differences are found between the estimates obtained with BAO data published by DESI and the BAO data collection used previously, although the DESI data narrow the intervals a little, might have a slight preference for alternative cosmologies, with a smaller amount of data. Finally, although in most of the statistical comparisons made with ΛCDM there is evidence in favor of the latter, it is never very strong and, in some cases of the Exponential and Hyperbolic Tangent models the evidence is in favor of the f(R) (weak and/or positive).

In summary, from the analyses carried out in this article it can be concluded that although these f(R) models cannot alleviate the H_0 tension completely and this is an issue to be studied, they continue to be promising and viable models for explaining the accelerated expansion of the late universe, with the additional feature of providing a clear proposal regarding the physics involved in this phenomenon—namely, unknown aspects of spacetime. This is an ambiguous issue in the standard context, as outlined in the first section, where it remains unclear whether it refers to exotic species or gravitational aspects, in addition to other interesting features from the perspective of theoretical physics exhibited by $f(R)$ theories.

VII. ACKNOWLEDGMENTS

The authors would like to thank D. Brout, M. Leizerovich, A. Ballatore and S. J. Landau for their helpful comments.

The authors are supported by CONICET Grant No. PIP 11220200100729CO, and Grants No.G175 from UNLP.

Appendix A: Methods for solving the Friedmann equations in specific $f(R)$ models

The solution of the Friedmann equations 7 often requires numerical integration, as analytical solutions are not generally feasible. To enhance computational efficiency and mitigate numerical instabilities, it is advantageous to tailor the methodology to the specific characteristics of each $f(R)$ model. Below, we outline the approaches used for the models under consideration.

1. Starobinsky and Hu-Sawicki Models

In order to optimize computational efficiency when solving the Friedmann equations, for the Hu-Sawicki and Starobinsky models we use the variable transformation proposed by de la Cruz-Dombriz *et al.* [25]. The set of variables is defined as:

$$x = \frac{\dot{R} f_{RR}}{H f_R}, \tag{A1a}$$

$$y = \frac{f}{6H^2 f_R}, \tag{A1b}$$

$$v = \frac{R}{6H^2}, \tag{A1c}$$

$$\Omega = \frac{8\pi G \rho_m}{3H^2 f_R}, \tag{A1d}$$

$$\Gamma = \frac{f_R}{R f_{RR}}, \tag{A1e}$$

$$r = R/R^*, \tag{A1f}$$

where $R^* = R_{HS}, R_S$ is a reference curvature scale. Using these variables, the field equations take the form:

$$\frac{\mathrm{d}H}{\mathrm{d}z} = \frac{H}{z+1}(2-v), \tag{A2a}$$

$$\frac{\mathrm{d}x}{\mathrm{d}z} = \frac{1}{z+1}\left(-\Omega - 2v + x + 4y + xv + x^2\right), \tag{A2b}$$

$$\frac{\mathrm{d}y}{\mathrm{d}z} = \frac{-1}{z+1}(vx\Gamma - xy + 4y - 2yv), \tag{A2c}$$

$$\frac{\mathrm{d}v}{\mathrm{d}z} = \frac{-v}{z+1}(x\Gamma + 4 - 2v), \tag{A2d}$$

$$\frac{\mathrm{d}\Omega}{\mathrm{d}z} = \frac{\Omega}{z+1}(-1 + 2v + x), \tag{A2e}$$

$$\frac{\mathrm{d}r}{\mathrm{d}z} = -\frac{x\Gamma r}{z+1}. \tag{A2f}$$

The redshift associated with the initial conditions for all models will correspond to the moment when the model

approaches the ΛCDM model closely enough, with which these conditions are calculated. This can be expressed as:

$$f(R(z_i)) = R - 2\Lambda(1-\epsilon)$$

With this condition, the following expression is derived [28]:

$$z_i = \left[\frac{4\Omega^{\Lambda}_{\Lambda,0}}{\Omega^{\Lambda}_{m_0}}\left(\frac{b}{4\nu_{f(R)}} - 1\right)\right]^{1/3} - 1, \tag{A3}$$

Where the expression for $\nu_{f(R)}$ in each model, as well as the assumed values for ϵ [28], are:

$$\nu_{hs} = \frac{1}{(1/\epsilon - 1)},\ \epsilon \approx 10^{-6} \tag{A4}$$

$$\nu_{st} = \left(\frac{1}{(1/\epsilon - 1)}\right)^{1/2},\ \epsilon \approx 10^{-8} \tag{A5}$$

$$\nu_{exp} = -\frac{1}{\ln \epsilon},\ \epsilon \approx 10^{-10} \tag{A6}$$

$$\nu_{tanh} = \frac{1}{\operatorname{arctanh}(1-\epsilon)},\ \epsilon \approx 10^{-10} \tag{A7}$$

$$\tag{A8}$$

Therefore, the initial conditions for Starobinsky and Hu Sawicki cases are given by:

$$x_i = 0 \tag{A9}$$

$$y_i = \frac{R_{\Lambda\mathrm{CDM}}(z_i) - 2\Lambda}{6H^2_{\Lambda\mathrm{CDM}}(z_i)} \tag{A10}$$

$$v_i = \frac{R_{\Lambda\mathrm{CDM}}(z_i)}{6H^2_{\Lambda\mathrm{CDM}}(z_i)} \tag{A11}$$

$$\Omega_i = 1 - v_i + x_i + y_i \tag{A12}$$

$$r_i = \frac{R_{\Lambda\mathrm{CDM}}(z_i)}{R_j} \tag{A13}$$

where $R_j = R_S$ or R_{HU}, depending on the case. $R_{\Lambda CDM}$ and $H_{\Lambda CDM}$ are the Ricci scalar and the Hubble function of the standard model, respectively.

Since the $f(R)$ model reduces to the standard model when $b = 0$, one can assume, as a solution for $H(z)$, a series expansion around the standard model solution, proposed by Basilakos *et al.* [71], valid only for small b, yielding a very low error.

$$H^2(N) = H^2_{\Lambda\mathrm{CDM}}(N) + \sum_{i=1}^{M} b^i \delta H^2_i(N), \tag{A14}$$

where $N = -\log(1+z)$.

This approach avoids numerical instabilities associated with $f_{RR} \to 0$. For cases with b smaller than a critical value b_{crit}, this solution is assumed, with a negligible error as indicated in [71]. For larger b, the full modified Friedmann equations 7 and 8 are solved numerically.

2. Exponential and Hyperbolic Tangent Models

For the exponential and hyperbolic tangent models meanwhile, we employ a different approach based on a redefinition of variables, which is presented in [24]. This method reformulates the Friedmann equations in terms of dimensionless variables, expressed as:

$$\frac{\mathrm{d}E}{\mathrm{d}x} = \Omega^{\Lambda\mathrm{CDM}}_{\Lambda,0}\frac{\mathcal{R}}{E} - 2E, \tag{A15a}$$

$$\frac{\mathrm{d}\mathcal{R}}{\mathrm{d}x} = \frac{2\Lambda}{f_{\mathcal{R}\mathcal{R}}}\left[\Omega^{\Lambda\mathrm{CDM}}_{m,0}\frac{a^{-3} + X^{\Lambda\mathrm{CDM}}a^{-4}}{E^2} - \frac{f_{\mathcal{R}}}{2\Lambda} + \frac{\mathcal{R}f_{\mathcal{R}} - f}{6\left(H^{\Lambda\mathrm{CDM}}_0\right)^2 E^2}\right], \tag{A15b}$$

where $E = H/H^{\Lambda\mathrm{CDM}}_0$,$X^{\Lambda CDM} = \frac{\Omega^{\Lambda CDM}_{r,0}}{\Omega^{\Lambda CDM}_{m,0}}$, $\mathcal{R} = R/(2\Lambda)$, and $x = -\log(1+z)$. $f_{\mathcal{R}}$ and $f_{\mathcal{R}\mathcal{R}}$ are the first and second derivatives with respect to $\mathcal{R}$.

The initial conditions for the exponential and hyperbolic tangent cases are given by:

$$E^2(x_i) = \Omega^{\Lambda\mathrm{CDM}}_{m,0}\left(e^{-3x_i} + X^{\Lambda\mathrm{CDM}}e^{-4x_i}\right) + \Omega^{\Lambda\mathrm{CDM}}_{\Lambda,0}, \tag{A16a}$$

$$\mathcal{R}(x_i) = 2 + \frac{\Omega^{\Lambda\mathrm{CDM}}_{m,0}}{2\Omega^{\Lambda\mathrm{CDM}}_{\Lambda,0}}e^{-3x_i}, \tag{A16b}$$

In most cases, the redshift calculated for the initial condition z_i is greater than the highest redshift in the observations, which we will denote as $z_{\max}$. For intermediate cases, where a value of b results in $z_i < z_{\max}$, the $f(R)$ model solution obtained from Eqs. A15a and A15b is assumed when $z < z_i$; while the standard solution Λ_{CDM} is considered in cases where $z_i < z$.

For parameter sets with extremely small b, z_i (Eq. A3) takes negative values, indicating that the model behaves indistinguishably from the standard model for all redshifts. Therefore, we assume Λ_{CDM} as a good approximation in such cases. This is very convenient since in the Exponential and Hyperbolic Tangent models, it is not possible to use a series expansion around the standard solution A14 as in the Starobinsky and Hu-Sawicki models, and in this methodology, the divergence $f_{RR} \to 0$ is also avoided.

[1] A. G. Riess, A. V. Filippenko, P. Challis, A. Clocchiatti, A. Diercks, P. M. Garnavich, R. L. Gilliland, C. J. Hogan, S. Jha, R. P. Kirshner, et al., Astron. J. **116**, 1009 (1998), astro-ph/9805201.

[2] S. Perlmutter, G. Aldering, G. Goldhaber, R. A. Knop, P. Nugent, P. G. Castro, S. Deustua, S. Fabbro, A. Goobar, D. E. Groom, et al., Astrophys. J. **517**, 565 (1999), astro-ph/9812133.

[3] A. G. Riess and L. Breuval, in *IAU Symposium*, edited by R. de Grijs, P. A. Whitelock, and M. Catelan (2024), vol. 376 of *IAU Symposium*, pp. 15–29, 2308.10954.

[4] Planck Collaboration, N. Aghanim, Y. Akrami, M. Ashdown, J. Aumont, C. Baccigalupi, M. Ballardini, A. J. Banday, R. B. Barreiro, N. Bartolo, et al., Astron. & Astrophys. **641**, A6 (2020), 1807.06209.

[5] A. Joyce, L. Lombriser, and F. Schmidt, Annual Review of Nuclear and Particle Science **66**, 95 (2016), 1601.06133.

[6] S. Tsujikawa, Classical and Quantum Gravity **30**, 214003 (2013), 1304.1961.

[7] E. J. Copeland, M. Sami, and S. Tsujikawa, International Journal of Modern Physics D **15**, 1753 (2006), hep-th/0603057.

[8] R. R. Caldwell and E. V. Linder, Physical Review Letters **95**, 141301 (2005), astro-ph/0505494.

[9] S. Weinberg, Reviews of Modern Physics **61**, 1 (1989).

[10] N. A. Bahcall, Science **284**, 1481 (1999), URL `https://doi.org/10.1126/science.284.5419.1481`.

[11] J. P. Ostriker and P. J. Steinhardt, Nature (London) **377**, 600 (1995).

[12] A. A. Starobinsky, Physics Letters B **91**, 99 (1980), ISSN 03702693.

[13] T. Asaka, S. Iso, H. Kawai, K. Kohri, T. Noumi, and T. Terada, Progress of Theoretical and Experimental Physics **2016**, 123E01 (2016), ISSN 2050-3911, https://academic.oup.com/ptep/article-pdf/2016/12/123E01/10436310/ptw161.pdf, URL `https://doi.org/10.1093/ptep/ptw161`.

[14] A. Cisterna, N. Grandi, and J. Oliva, Phys. Rev. D **110**, 084043 (2024), 2406.10037.

[15] M. Artymowski and Z. Lalak, JCAP **09**, 036 (2014), 1405.7818.

[16] S. Nojiri and S. D. Odintsov, TSPU Bulletin **N8(110)**, 7 (2011), 0807.0685.

[17] . D.Perez, et al., *New Phenomena and New States of Matter in the Universe* (2023).

[18] R. H. Dicke, Physical Review **125**, 2163 (1962).

[19] S. Capozziello, R. de Ritis, and A. A. Marino, Classical and Quantum Gravity **14**, 3243 (1997), gr-qc/9612053.

[20] S. Capozziello, P. Martin-Moruno, and C. Rubano, Physics Letters B **689**, 117 (2010), 1003.5394.

[21] J. Park and T. H. Lee, Mod. Phys. Lett. A **38**, 2350047 (2023).

[22] B. Hu, M. Raveri, M. Rizzato, and A. Silvestri, Mon. Not. R. Astron. Soc. **459**, 3880 (2016), 1601.07536.

[23] . Nunes et al., Journal of Cosmology and Astroparticle Physics **2017**, 005 (2017), URL `https://doi.org/10.1088%2F1475-7516%2F2017%2F01%2F005`.

[24] S. D. Odintsov, D. Sáez-Chillón Gómez, and G. S. Sharov, Eur. Phys. J. C **77**, 862 (2017).

[25] Á. de la Cruz-Dombriz, P. K. S. Dunsby, S. Kandhai, and D. Sáez-Gómez, Phys. Rev. D **93**, 084016 (2016), 1511.00102.

[26] M. Leizerovich, L. Kraiselburd, S. Landau, and C. G. Scóccola, Physical Review D **105**, 103526 (2022), 2112.01492.

[27] S. D. Odintsov, D. Sáez-Chillón Gómez, and G. S. Sharov, Nuclear Physics B **966**, 115377 (2021), ISSN 0550-3213, URL `https://www.sciencedirect.com/science/article/pii/S0550321321000742`.

[28] C. R. Farrugia, J. Sultana, and J. Mifsud, Phys. Rev. D **104**, 123503 (2021), 2106.04657.

[29] K. Ravi, A. Chatterjee, B. Jana, and A. Bandyopadhyay, Monthly Notices of the Royal Astronomical Society **527**, 7626 (2024), 2306.12585.

[30] R. Kou, C. Murray, and J. G. Bartlett, Astron. & Astrophys. **686**, A193 (2024), 2311.09936.

[31] S. Li, A. G. Riess, D. Scolnic, S. Casertano, and G. S. Anand, arXiv e-prints arXiv:2502.05259 (2025), 2502.05259.

[32] L. Amendola and S. Tsujikawa, *Dark Energy: Theory and Observations* (2010).

[33] A. De Felice and S. Tsujikawa, Living Reviews in Relativity **13**, 3 (2010), 1002.4928.

[34] W. Hu and I. Sawicki, Phys. Rev. D **76**, 064004 (2007), 0705.1158.

[35] G. Cognola, E. Elizalde, S. Nojiri, S. D. Odintsov, L. Sebastiani, and S. Zerbini, Phys. Rev. D **77**, 046009 (2008), URL `https://link.aps.org/doi/10.1103/PhysRevD.77.046009`.

[36] S. Tsujikawa, Physical Review D **77** (2008), ISSN 1550-2368, URL `http://dx.doi.org/10.1103/PhysRevD.77.023507`.

[37] J. Simon, L. Verde, and R. Jimenez, Phys. Rev. D **71**, 123001 (2005), astro-ph/0412269.

[38] D. Stern, R. Jimenez, L. Verde, M. Kamionkowski, and S. A. Stanford, JCAP **2**, 008 (2010), 0907.3149.

[39] M. Moresco, A. Cimatti, R. Jimenez, L. Pozzetti, G. Zamorani, M. Bolzonella, J. Dunlop, F. Lamareille, M. Mignoli, H. Pearce, et al., JCAP **8**, 006 (2012), 1201.3609.

[40] C. Zhang, H. Zhang, S. Yuan, S. Liu, T.-J. Zhang, and Y.-C. Sun, Research in Astronomy and Astrophysics **14**, 1221-1233 (2014), 1207.4541.

[41] M. Moresco, Mon. Not. R. Astron. Soc. **450**, L16 (2015), 1503.01116.

[42] M. Moresco, L. Pozzetti, A. Cimatti, R. Jimenez, C. Maraston, L. Verde, D. Thomas, A. Citro, R. Tojeiro, and D. Wilkinson, JCAP **5**, 014 (2016), 1601.01701.

[43] N. Borghi, M. Moresco, and A. Cimatti, The Astrophysical Journal Letters **928**, L4 (2022), URL `https://dx.doi.org/10.3847/2041-8213/ac3fb2`.

[44] D. Brout, D. Scolnic, and et al., The Astrophys. Journal **938**, 110 (2022), 2202.04077.

[45] D. Scolnic, D. Brout, A. Carr, and et al., The Astrophys. Journal **938**, 113 (2022), 2112.03863.

[46] A. G. Riess, W. Yuan, L. M. Macri, D. Scolnic, D. Brout, S. Casertano, D. O. Jones, Y. Murakami, G. S. Anand, L. Breuval, et al., Astrophys. J. Lett. **934**, L7 (2022), 2112.04510.

[47] A. Conley, J. Guy, M. Sullivan, N. Regnault, P. Astier, C. Balland, S. Basa, R. G. Carlberg, D. Fouchez,

D. Hardin, et al., Astropys. Journal Suppl. **192**, 1 (2011), 1104.1443.

[48] D. Camarena and V. Marra, Physical Review Research **2**, 013028 (2020), 1906.11814.

[49] D. Camarena and V. Marra, arXiv e-prints arXiv:2307.02434 (2023), 2307.02434.

[50] A. T. Chantada, S. J. Landau, P. Protopapas, C. G. Scóccola, and C. Garraffo, Phys. Rev. D **107**, 063523 (2023), 2205.02945.

[51] A. T. Chantada, S. J. Landau, P. Protopapas, C. G. Scóccola, and C. Garraffo, Phys. Rev. D **109**, 123514 (2024), URL https://link.aps.org/doi/10.1103/PhysRevD.109.123514.

[52] W. L. Freedman, B. F. Madore, I. S. Jang, T. J. Hoyt, A. J. Lee, and K. A. Owens, arXiv e-prints arXiv:2408.06153 (2024), 2408.06153.

[53] L. Perivolaropoulos, Phys. Rev. D **110**, 123518 (2024), 2408.11031.

[54] A. J. Ross, L. Samushia, C. Howlett, W. J. Percival, A. Burden, and M. Manera, Monthly Notices of the Royal Astronomical Society **449**, 835–847 (2015), ISSN 0035-8711, URL http://dx.doi.org/10.1093/mnras/stv154.

[55] J. E. Bautista, N. G. Busca, J. Guy, J. Rich, M. Blomqvist, H. du Mas des Bourboux, M. M. Pieri, A. Font-Ribera, S. Bailey, T. Delubac, et al., Astronomy and Astrophysics **603**, A12 (2017), ISSN 1432-0746, URL http://dx.doi.org/10.1051/0004-6361/201730533.

[56] J. E. Bautista, R. Paviot, M. Vargas Magaña, S. de la Torre, S. Fromenteau, H. Gil-Marín, A. J. Ross, E. Burtin, K. S. Dawson, J. Hou, et al., Monthly Notices of the Royal Astronomical Society **500**, 736–762 (2020), ISSN 1365-2966, URL http://dx.doi.org/10.1093/mnras/staa2800.

[57] R. Neveux, E. Burtin, A. de Mattia, A. Smith, A. J. Ross, J. Hou, J. Bautista, J. Brinkmann, C.-H. Chuang, K. S. Dawson, et al., Mon. Not. R. Astron. Soc. **499**, 210 (2020), 2007.08999.

[58] M. Ata, F. Baumgarten, J. Bautista, F. Beutler, D. Bizyaev, M. R. Blanton, J. A. Blazek, A. S. Bolton, J. Brinkmann, J. R. Brownstein, et al., Monthly Notices of the Royal Astronomical Society **473**, 4773–4794 (2017), ISSN 1365-2966, URL http://dx.doi.org/10.1093/mnras/stx2630.

[59] S. Alam, M. Ata, S. Bailey, F. Beutler, D. Bizyaev, J. A. Blazek, A. S. Bolton, J. R. Brownstein, A. Burden, C.-H. Chuang, et al., Monthly Notices of the Royal Astronomical Society **470**, 2617–2652 (2017), ISSN 1365-2966, URL http://dx.doi.org/10.1093/mnras/stx721.

[60] H. du Mas des Bourboux, J.-M. Le Goff, M. Blomqvist, N. G. Busca, J. Guy, J. Rich, C. Yèche, J. E. Bautista, E. Burtin, K. S. Dawson, et al., Astronomy and Astrophysics **608**, A130 (2017), ISSN 1432-0746, URL http://dx.doi.org/10.1051/0004-6361/201731731.

[61] T. M. C. Abbott, F. B. Abdalla, A. Alarcon, S. Allam, F. Andrade-Oliveira, J. Annis, S. Avila, M. Banerji, N. Banik, K. Bechtol, et al., Monthly Notices of the Royal Astronomical Society **483**, 4866–4883 (2018), ISSN 1365-2966, URL http://dx.doi.org/10.1093/mnras/sty3351.

[62] E. A. Kazin, J. Koda, C. Blake, N. Padmanabhan, S. Brough, M. Colless, C. Contreras, W. Couch, S. Croom, D. J. Croton, et al., Monthly Notices of the Royal Astronomical Society **441**, 3524–3542 (2014), ISSN 0035-8711, URL http://dx.doi.org/10.1093/mnras/stu778.

[63] A. G. Adame, J. Aguilar, S. Ahlen, S. Alam, D. M. Alexander, M. Alvarez, O. Alves, A. Anand, U. Andrade, E. Armengaud, et al., JCAP **2025**, 021 (2025), 2404.03002.

[64] H. Akaike, IEEE Transactions on Automatic Control **19**, 716 (1974).

[65] G. Schwarz, The Annals of Statistics **6**, 461 (1978), URL https://doi.org/10.1214/aos/1176344136.

[66] K. P. Burnham and D. R. Anderson, Sociological Methods & Research **33**, 261 (2004), https://doi.org/10.1177/0049124104268644, URL https://doi.org/10.1177/0049124104268644.

[67] . Bevington et al., *Data Reduction and Error Analysis for the Physical Sciences* (1969).

[68] A. R. Liddle, Mon. Not. R. Astron. Soc. **351**, L49 (2004), astro-ph/0401198.

[69] S. D. Odintsov, D. Sáez-Chillón Gómez, and G. S. Sharov, arXiv e-prints arXiv:2412.09409 (2024), 2412.09409.

[70] S. Kumar, R. C. Nunes, S. Pan, and P. Yadav, Phys. Dark Univ. **42**, 101281 (2023), 2301.07897.

[71] S. Basilakos, S. Nesseris, and L. Perivolaropoulos, Phys. Rev. D **87**, 123529 (2013), URL https://link.aps.org/doi/10.1103/PhysRevD.87.123529.

[72] L. Perivolaropoulos and F. Skara, Monthly Notices of the Royal Astronomical Society **520**, 5110 (2023), ISSN 0035-8711, https://academic.oup.com/mnras/article-pdf/520/4/5110/54034587/stad451.pdf, URL https://doi.org/10.1093/mnras/stad451.

[73] A. G. Riess, D. Scolnic, G. S. Anand, L. Breuval, S. Casertano, L. M. Macri, S. Li, W. Yuan, C. D. Huang, S. Jha, et al., Astrophys. J. **977**, 120 (2024), 2408.11770.

[74] D. Scolnic, P. Boubel, J. Byrne, A. G. Riess, and G. S. Anand, arXiv e-prints arXiv:2412.08449 (2024), 2412.08449.